parameter analyser, connected to the HBTs via a vacuum compatible biaxial feedthrough, and controlled by software by ICS.

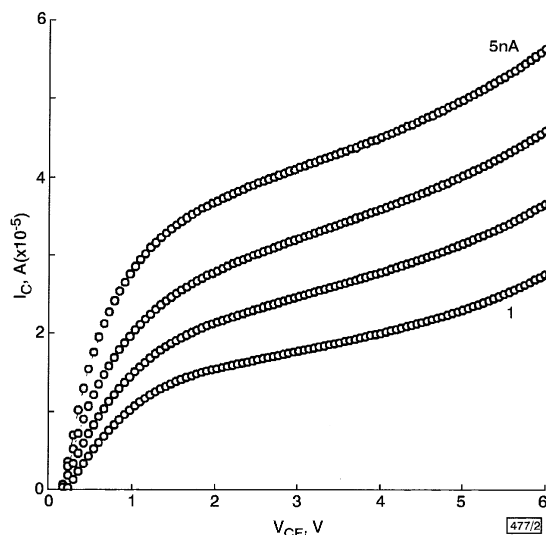

Fig. 2 *Phototransistor I-V curves from npn AlGaN/GaN HBT*

Results and discussion: Fig. 2 shows a family of I-V curves from a transistor under investigation. One can see from this Figure that the nA-range current of electron beam, injected in the base, can control the μA-range collector current, while the collector-emitter voltage varies from 0 to 6 V. The I-V curves in Fig. 2 correspond to the common emitter testing configuration.

The amplification coefficient β of the phototransistor can be calculated, as explained in [2 – 4], according to

$$\beta = \frac{\Delta I_{EC}}{\Delta I_B G} \quad (1)$$

where ΔI_{EC} is the difference between currents (collector-emitter) through the structure at different values of I_B; ΔI_B is the difference between beam currents; G is the generation factor, which is the electron-hole pair generation rate per unit volume. G was obtained based on the ionisation energy, consumed per electron-hole pair, as a function of the bandgap energy [5]. Since it takes ~10 eV for electron-hole pair generation in GaN, we concluded that the value of G is ~3000 at 30 kV acceleration voltage. Determining the value of ΔI_{EC} at 5 V (the curves corresponding to I_B of 1 and 5 nA were used), and inserting the value of G into eqn. 1, we obtained $\beta \simeq 2.5$ for an HBT under investigation. This value is in good agreement with β values measured using three-terminal conventional measurements [1]. This is a strong argument in favour of the validity of the phototransistor measurements.

Conclusions: Phototransistor measurements were carried out in AlGaN/GaN HBTs *in situ* in a scanning electron microscope. SEM electron beam current was used in these measurements as an analogue of base current. The measurements are in good agreement with the three-terminal counterpart. This indicates that the phototransistor technique may be used as an express method to monitor amplification without fabricating an ohmic contact to the *p*-type base of an AlGaN/GaN HBT.

Acknowledgments: This research was supported in part by the UCF start-up grant and at UF by DMR 0101438 and CTS 117399.

© IEE 2001
11 September 2001
Electronics Letters Online No: 20010948
DOI: 10.1049/el:20010948

L. Chernyak (*Physics Department, University of Central Florida, Orlando, FL 32816-2385, USA*)

E-mail: chernyak@physics.ucf.edu

A. Osinsky (*Corning Applied Technologies, Woburn, MA 01801, USA*)

S.J. Pearton (*Department of Materials Science and Engineering, University of Florida, Gainesville, FL 32611, USA*)

F. Ren (*Department of Chemical Engineering, University of Florida, Gainesville, FL 32611, USA*)

References

1 PEARTON, S.J., REN, F., ZHANG, A.P., and LEE, K.P.: 'Fabrication and performance of GaN electronic devices', *Mater. Sci. Eng.*, 2000, **R30**, pp. 55–212 (See also special issue of *IEEE Trans. Electron. Devices*, MISHRA, U.K., and ZOLPER, J.C. (Eds.), 2001, **48**, pp. 405–608)

2 CAHEN, D., GILET, J.-M., SCHMITZ, C., CHERNYAK, L., GARTSMAN, K., and JAKUBOWICZ, A.: 'Room-temperature, electric field-induced creation of stable devices in $CuInSe_2$ crystals', *Science*, 1992, **258**, pp. 271–274

3 CHERNYAK, L., LYAKHOVITSKAYA, V., RICHTER, S., JAKUBOWICZ, A., MANASSEN, Y., COHEN, S.R., and CAHEN, D.: 'Electronic effects of ion mobility in semiconductors: mixed electronic-ionic behavior and device creation in Si:Li', *J. Appl. Phys.*, 1996, **80**, pp. 2749–2762

4 CHERNYAK, L., LYAKHOVITSKAYA, V., and CAHEN, D.: 'Low temperature device creation in Si via fast Li electromigration', *Appl. Phys. Lett.*, 1995, **66**, pp. 709–711

5 LEAMY, H.J.: 'Charge collection scanning electron microscopy', *J. Appl. Phys.*, 1982, **53**, pp. R51–R80

pnp Si resonant interband tunnel diode with symmetrical NDR

N. Jin, P.R. Berger, S.L. Rommel, P.E. Thompson and K.D. Hobart

A Si-based resonant interband tunnel diode (RITD) is presented with a *pnp* configuration so that an integrated RITD can be easily used to form a latch. The I-V characteristics of this *pnp* RITD show symmetrical negative differential resistance (NDR) regions in both forward and reverse bias. The top diode shows a peak-to-valley current ratio (PVCR) of 1.63 with peak current density (J_p) of 1.5 kA/cm², while the bottom diode shows a PVCR of 1.51 with J_p of 2.0 kA/cm².

Introduction: Since the development of Si-based resonant interband tunnelling diodes (RITD) [1] that can potentially be integrated with CMOS transistors for highly functional tunnel diode-transistor circuits [2], numerous experimental attempts have been made to improve RITD performance [3, 4]. A latch can be formed by two serially-connected Esaki tunnel diodes [5] or by two back-to-back resonant tunnelling diodes (RTD) [6]. A concern for any monolithic interband tunnel diode technology with all devices oriented in the same direction, including existing Si-based RITD based on *n*-on-*p* or *p*-on-*n* configurations, is the difficulty to create a latch with back-to-back interband tunnel diodes that employ a single *p*-*n* junction. This is because, unlike an RTD that exhibits symmetrical I-V characteristics, an RITD is an interband tunnel diode and therefore exhibits negative differential resistance (NDR) only under one bias condition and a short circuit in the reverse. Therefore, two interband tunnel diode NDR regions would not intersect without cumbersome interconnect wiring. This could be solved by integrating both *n*-on-*p* and *p*-on-*n* RITDs into the same CMOS circuit, or by building a hybrid tunnel diode that exhibits symmetrical I-V characteristics. III-V-based RITDs using a symmetric *pnp* configuration have reported two NDR regions [7] but, to our knowledge, symmetrical NDR has not been reported in Si-based interband tunnelling diodes. This Letter presents the first working *pnp* Si-based RITD by using a growth technique to mimic the performance of an RTD, so that it exhibits NDR in both forward and reverse bias.

Experiment: Given the fact that the NDR regions appear in the opposite bias direction for *p*-on-*n* and *n*-on-*p* RITDs, it is natural to design a *pnp* or *npn* RITD by combining *p*-on-*n* and *n*-on-*p* RITD back-to-back so that the I-V characteristics of the *pnp* RITD will exhibit NDR in both forward and reverse bias. However, this must be done in such a way that the performance of each is not seriously sacrificed. Segregation of dopants is of primary concern [8]. Fig. 1 shows schematic diagrams of *n*-on-*p* and *p*-on-*n* structures used in previous studies [3, 9]. The *p*-on-*n* struc-

ture is designed to control the Sb segregation, because Sb incorporated into the intrinsic tunnelling spacer would result in unintentional doping, and hence a lower peak-to-valley current ratio (PVCR). The previous study [9] on Si-based *p*-on-*n* RITDs with this structure showed that by setting $L1$ as 5 nm and $L2$ as 3 nm, a PVCR of 1.7 with J_p of 2.6 kA/cm^2 could be obtained. Depositing the Sb δ-doping plane and a Si spacer of thickness $L1$, equal to 5 nm, at 320°C minimised the segregation, and ensured that a large percentage of dopants incorporate into the lattice. The growth was then stopped and the substrate temperature was altered for the growth of the next layer. Rather than dropping the substrate temperature to suppress Sb segregation further, the substrate temperature was elevated to promote segregation of the remaining Sb, while concurrently minimising Sb incorporation into the tunnel barrier. A second Si spacer of thickness $L2$, equal to 3 nm, is then grown at elevated temperature before the next δ-doping spike is inserted. The effective tunnelling spacer, as measured by secondary ion mass spectroscopy (SIMS) and confirmed by I-V measurements, is not 8 nm, but 6 nm. Additionally, we have found that optimisation of the post-growth rapid thermal annealing (RTA) conditions (575°C, 1 mm) on *p*-on-*n* 5 nm/3 nm RITD increased the PVCR to 2.1 with J_p of 1.1 kA/cm^2. These performance parameters are comparable to the best performance of an *n*-on-*p* RITD with 6 nm undoped Si spacer [3]. Fig. 2 shows the comparison of the I-V characteristics of these *p*-on-*n* and *n*-on-*p* RITDs. Note the NDR regions appear inverted to each other as expected.

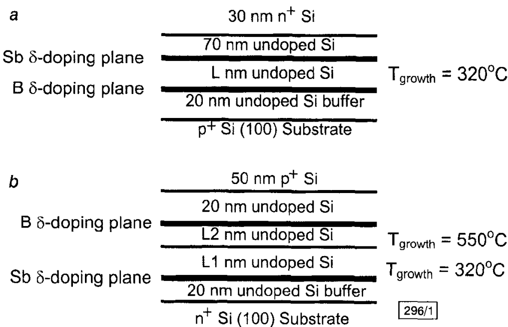

Fig. 1 *Schematic diagram of n-on-p and p-on-n RITD structures*

a *n*-on-*p* RITD
Best performance achieved when $L = 6$ nm
b *p*-on-*n* RITD
Best performance achieved when $L1 = 5$ nm, $L2 = 3$ nm

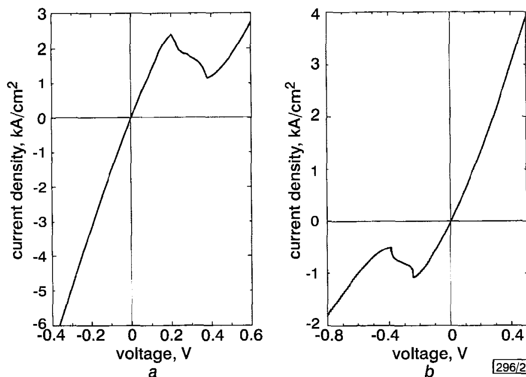

Fig. 2 *Comparison of I-V characteristics of n-on-p RITD and p-on-n RITD*

a *n*-on-*p* RITD
b *p*-on-*n* RITD

Based on these results, the *pnp* structure shown in Fig. 3 was designed by combining the *p*-on-*n* (5 nm/3 nm) RITD structure and the *n*-on-*p* (6 nm) structure to obtain the highest PVCR while maintaining the symmetry of the I-V characteristics. Epitaxial growth was achieved with a specially designed molecular beam epitaxy (MBE) growth system using elemental Si in an electron-beam source. The structures were grown on 75 mm B-doped (ρ = 0.015–0.04 Ω·cm) Si (100) wafers. After the growth of a Si buffer at 650°C, the substrate temperature was lowered. The first B δ-doping plane was deposited while the substrate was cooling from 450 to 320°C. The 6 nm Si spacer, the Sb δ-doping plane, and the 5 nm Si spacer were grown at 320°C. The Si flux was then terminated while the substrate temperature was elevated to 550°C for the remainder of the sample growth, including the deposition of the second B δ-doping plane. Prior to device fabrication, portions of the wafers were annealed using a forming gas ambient in an AG Associates HeatPulse 610 RTA furnace at various temperatures for 1 min. Ti/Au dots with 18 μm diameters were patterned on the surface of the wafers via a standard contact lithography. A buffered oxide etch was used prior to metallisation. Using the Ti/Au dots as a self-aligned mask, CF_4/O_2 plasma etching was performed to get the diode mesa. Finally, a Ti/Au backside contact was thermally evaporated on all of the samples.

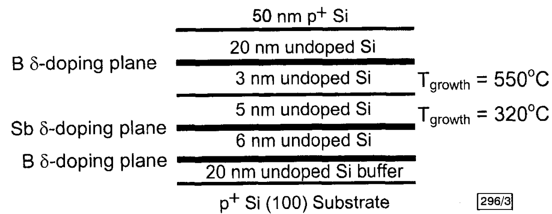

Fig. 3 *Schematic diagram of pnp RITD structure developed for symmetrical NDR regions*

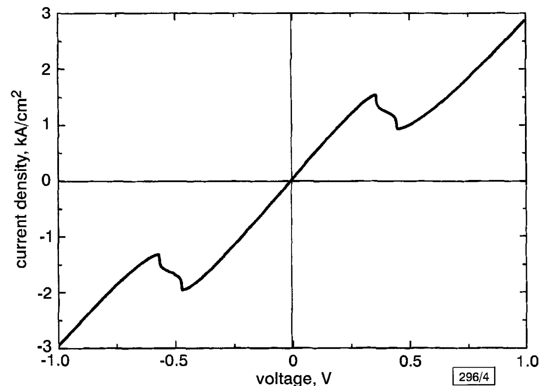

Fig. 4 *I-V characteristic of pnp RITD clearly showing NDR present in both forward and reverse bias directions*

Results: Fig. 4 shows the I-V characteristics of a *pnp* RITD after a 600°C, 1 min RTA. The optimum anneal temperature for the *pnp* RITD is a compromise between the optimum anneal temperatures for the individual *p*-on-*n* and *n*-on-*p* RITD. Note that when a forward bias is applied, the device nearer the surface (the top diode) will be under forward bias, and when a reverse bias is applied with respect to the layers, the device nearer the substrate (the bottom diode) will be under forward bias. As expected, NDR is clearly present in the forward and reverse directions with a PVCR of 1.63 for the top diode and 1.51 for the bottom diode. A symmetric I-V characteristic is clearly present as the current density of the bottom diode (1.5 kA/cm^2) is about the same as that of the top diode (2.0 kA/cm^2).

Conclusion: By careful control of the growth temperatures, we were able to combine the *p*-on-*n* and *n*-on-*p* growth templates to form a new Si-based tunnel diode structure. The Si *pnp* RITD fabrication process is compatible with the thermal budget of CMOS transistors, making it suitable for integration to form tunnel diode logic circuits.

Acknowledgments: The authors wish to thank D.S. Simons of the National Institute of Standards and Technology for SIMS of the *n*-on-*p* and *p*-on-*n* RITDs and T.E. Dillon, S. Di Giacomo, B. Cord and C. D'Imperio, of the University of Delaware, Department of Electrical and Computer Engineering for assistance in fabrication and testing.

© IEE 2001
17 August 2001
Electronics Letters Online No: 20010961
DOI: 10.1049/el:20010961

N. Jin and P.R. Berger (*Ohio State University, Department of Electrical and Computer Engineering, Columbus, OH 43210 USA*)

E-mail: pberger@ieee.org

S.L. Rommel (*University of Illinois, Department of Electrical and Computer Engineering, Urbana, IL 61801 USA*)

P.E. Thompson and K.D. Hobart (*Naval Research Laboratory, Code 6812, Washington, DC 20375-5347, USA*)

References

1 ROMMEL, S.L., DILLON, T.E., DASHIELL, M.W., FENG, H., KOLODZEY, J., BERGER, P.R., THOMPSON, P.E., HOBART, K.D., LAKE, R., SEABAUGH, A.C., KLIMECK, G., and BLANKS, D.K.: 'Room temperature operation of epitaxially grown $Si/Si_{0.59}Ge_{0.5}/Si$ resonant interband tunneling diodes', *Appl. Phys. Lett.*, 1998, **73**, pp. 2191–2193

2 SEABAUGH, A., BRAR, B., BROEKAERT, T., LAKE, R., MORRIS, F., FRAZIER, G., DENG, X., and BLAKE, T.: 'Transistors and tunnel diodes for analog/mixed-signal circuits and embedded memory'. Int. Electron Device Meet. Tech. Dig., 1998, pp. 429–432

3 THOMPSON, P.E., HOBART, K.D., TWIGG, M., JERNIGAN, G., DILLON, T.E., ROMMEL, S.L., BERGER, P.R., SIMONS, D.S., LAKE, R., and SEABAUGH, A.C.: 'Si resonant interband tunnel diodes grown by low temperature molecular beam epitaxy', *Appl. Phys. Lett.*, 1999, **75**, pp. 1308–1310

4 DUSCHL, R., SCHMIDT, O.G., REITEMANN, G., KASPER, E., and EBERL, K.: 'High room temperature peak-to-valley current ratio in Si-based Esaki diodes', *Electron. Lett.*, 1999, **35**, pp. 1111–1112

5 GOTO, E., MUTARA, K., NAKAZAWA, K., MOTO-OKA, T., MATSUOKA, Y., ISHIBASHI, Y., SOMA, T., and WADA, E.: 'Esaki diode high-speed logical circuits', *IRE Trans. Electron. Comput.*, 1960, **9**, pp. 25–29

6 VAN DER WAGT, J.P.A.: 'Tunneling-based SRAM', *Proc. IEEE*, 1999, **87**, pp. 571–595

7 WANG, Y.H.: 'Interband resonant tunneling diode in δ-doped GaAs', *Appl. Phys. Lett.*, 1990, **57**, pp. 1546–1547

8 HOBART, K.D., GODBEY, D.J., TWIGG, M.E., FATEMI, M., THOMPSON, P.E., and SIMONS, D.S.: 'Surface segregation and structure of Sb-doped Si(100) films grown at low temperature by molecular beam epitaxy', *Surf. Sci.*, 1995, **334**, pp. 29–38

9 HOBART, K.D., THOMPSON, P.E., ROMMEL, S.L., DILLON, T.E., BERGER, P.R., SIMONS, D.S., and CHI, P.H.: 'A p-on-n Si interband tunnel diode grown by molecular beam epitaxy', *J. Vac. Sci. Technol. B*, 2001, **19**, pp. 290–293

Algebraic differential decorrelation for nonstationary source separation

Seungjin Choi and A. Cichocki

A differential correlation is introduced which is able to capture the time-varying statistics of nonstationary signals and it is shown that minimisation of differential cross-correlations between observation signals can achieve nonstationary source separation. For implementation, an algebraic method is employed, the joint approximate diagonalisation, therefore the resulting method is referred to as Algebraic Differential DEcorrelation (ADDE). The useful behaviour of the method is confirmed by computer simulations.

Introduction: Source separation is a fundamental problem that is encountered in many practical applications such as telecommunications, image/speech processing, and biomedical signal analysis where multiple sensors are involved. In its simplest form, the m-dimensional observation vector $\mathbf{x}(t) \in \mathbb{R}^m$ is assumed to be generated by

$$\mathbf{x}(t) = \mathbf{A}\mathbf{s}(t) \qquad (1)$$

where $\mathbf{A} \in \mathbb{R}^{m \times n}$ is the unknown mixing matrix, $\mathbf{s}(t)$ is the n-dimensional source vector (which is also unknown and $n \leq m$).

In this Letter, we consider the case where sources are nonstationary (especially second-order nonstationary in the sense that their variances are time-varying) [1]. In such a case, it might be useful to exploit the information on how fast the correlations between signals are changing. To this end, we introduce a concept of differential correlation and present an Algebraic Differential DEcorrelation (ADDE) method for nonstationary source separation. For simplicity we assume that sources have zero mean, but this is not necessary for our algorithm.

Differential correlation: A differential statistic is defined by the derivative of statistic with respect to time (or its discrete-time counterpart is defined by the difference between statistics) and is closely related to the differential learning [2, 3]. We define the time-delayed correlation matrix of the observation vector $\mathbf{x}(t)$ by

$$\mathbf{R}_x(t_k, \tau) = E\{\mathbf{x}(t_k)\mathbf{x}^T(t_k - \tau)\} \qquad (2)$$

In practice, the sample correlation matrix $\hat{\mathbf{R}}_x(t_k, \tau)$ is computed using the samples in the kth time-windowed data frame. Here we use the notation $\mathbf{R}_x(t_k, \tau)$ for both ensemble correlation and sample correlation.

The differential correlation matrix is defined by

$$\delta\mathbf{R}_x(t, \tau) = \frac{\partial \mathbf{R}_x(t, \tau)}{\partial t} \qquad (3)$$

or, its discrete-time counterpart is defined by

$$\delta\mathbf{R}_x(t_k, t_l, \tau) = \mathbf{R}_x(t_k, \tau) - \mathbf{R}_x(t_l, \tau) \qquad (4)$$

The definition in eqn. 4 will be used hereafter.

One can easily see that the linear data model, eqn. 1, has the following decomposition:

$$\delta\mathbf{R}_x(t_k, t_l, \tau) = \mathbf{A}\delta\mathbf{R}_s(t_k, t_l, \tau)\mathbf{A}^T \qquad \text{for } t_k \neq t_l \qquad (5)$$

where $\delta\mathbf{R}_s(t_k, t_l, \tau)$ is the differential correlation matrix of source vector $\mathbf{s}(t)$ that is assumed to be a diagonal matrix. It follows from eqn. 5 that the mixing matrix $\mathbf{A}$ can be estimated by solving a generalised eigenvalue problem

$$\delta\mathbf{R}_x(t_2, t_3, 0)\mathbf{U} = \delta\mathbf{R}_x(t_1, t_2, 0)\mathbf{U}\mathbf{\Lambda} \qquad (6)$$

where $\mathbf{U}$ and $\mathbf{\Lambda}$ correspond to the eigenvector and eigenvalue matrices, respectively. In such a case, the mixing matrix is given by $\mathbf{A} = \mathbf{U}^{-T}$. However, this is a valid solution only if all the diagonal elements of $\mathbf{\Lambda}$ are distinct. To avoid this difficulty, we exploit multiple differential correlation matrices and apply the joint approximate diagonalisation method to estimate the mixing matrix. This is described in the following Section.

Algorithm: ADDE: First we whiten the data $\mathbf{x}(t)$ to obtain $\mathbf{z}(t) = \mathbf{Q}\mathbf{x}(t)$ where $\mathbf{Q}$ is a whitening transformation. We then have

$$\mathbf{z}(t) = \mathbf{Q}\mathbf{A}\mathbf{s}(t) = \mathbf{B}\mathbf{s}(t) \qquad (7)$$

where $\mathbf{B} \in \mathbb{R}^{n \times n}$ is an orthogonal matrix, i.e. $\mathbf{B}\mathbf{B}^T = \mathbf{I}$. The whitened vector $\mathbf{z}(t)$ then satisfies

$$\delta\mathbf{R}_z(t_i, t_{i+1}, \tau_j) = \mathbf{B}\delta\mathbf{R}_s(t_i, t_{i+1}, \tau_j)\mathbf{B}^T \qquad (8)$$

Note that it is not necessary to exploit two adjacent data frames to compute the differential correlation matrix, but here we show just one exemplary case.

We apply the joint approximate diagonalisation to estimate the unitary mixing matrix $\mathbf{B}$, as in JADE [4], SOBI [5], and SEONS [6]. The algorithm ADDE is summarised below.

Algorithm outline: ADDE:

(i) Pre-whiten the observation data using whole data points so that the whitened data $\mathbf{z}(t) = \mathbf{Q}\mathbf{x}(t)$ is a unitary mixture of sources (where $\mathbf{Q}$ is a whitening transformation).

(ii) Divide the data $\{\mathbf{z}(t)\}$ into K non-overlapping blocks and calculate $(K-1)J$ differential correlation matrices, $\delta R_z(t_i, t_{i+1}, \tau_j)$ for $i = 1, ..., K-1$ and $j = 1, ..., J$ (e.g. $\tau_j = j - 1$).

(iii) Find a unitary joint diagonaliser $\mathbf{V}$ of $\{\delta\mathbf{R}_z(t_i, t_{i+1}, \tau_j)\}$ which satisfies

$$\mathbf{V}^T\delta\mathbf{R}_z(t_i, t_{i+1}, \tau_j)\mathbf{V} = \mathbf{\Lambda}_{i,j} \qquad (9)$$

where $\{\mathbf{\Lambda}_{i,j}\}$ is a set of diagonal matrices.

(iv) The demixing matrix is given by $\mathbf{W} = \mathbf{V}^T\mathbf{Q}$.

Numerical example: In this simulation, we used one digitised voice signal, one digitised music signal (both of which were sampled at 8 kHz), and three Gaussian signals with no temporal correlations but their variances being time-varying. The mixture vector $\mathbf{x}(t)$